# NE 533 MOOSE Project: Part 3

**Alexandra Doherty**
04.25.2025

## Abstract

Understanding the thermal behavior of fuel rods in a nuclear reactor environment is imperative for the knowledge of how to safely operate nuclear power plants. In order to tabulate the temperature profiles of fuel rods, we first simulate a single fuel pellet behavior with a steady-state linear heat rate and a transient linear heat rate, with both constant, and temperature-dependent thermal conductivity values in the fuel, gap, and cladding using INL's MOOSE Framework[4].

## Introduction

The goal of this report is to outline temperature profiles of nuclear fuel using the MOOSE Framework. The prompt of the first portion of these simulations is based on the fuel pellet shown in the figure below. The height of the pellet is 1.0 cm, the $R_f$ is 0.5 cm, the $R_g$ is 0.005 cm, and the $R_c$ is 0.1 cm.

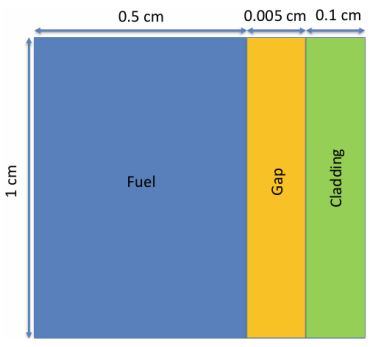


Figure 1: This figure shows the dimensions of the fuel pellet outlined in the proposal of this simulation design.

Five separate conditions were to be simulated:

- Steady-state linear heat rate with a constant thermal conductivity
- Steady-state linear heat rate with a temperature-dependent thermal conductivity
- Transient linear heat rate with a constant thermal conductivity
- Transient linear heat rate with a temperature-dependent thermal conductivity
- Steady-state linear heat rate with a temperature and burnup dependent thermal conductivity

The second part of these simulations involved extending the fuel to 1 m, while maintaining all other dimensions. This represents a 2D Axisymmetric fuel rod with smeared pellets, and enables the computation of axial temperature profiles. In this case, we highlight the temperature profiles of the fuel centerline, fuel surface, and inner cladding.

The third component of these simulations includes the same setup as part 1, using a temperature and burnup dependent thermal conductivity, constant linear heat rate, includes effects of thermal expansion, densification, and fission product (FP) induced swelling. This is simulated until gap closure and the goal is to determine displacements and stress state in the fuel as a function of time, and analyze thermal stresses cracks in the fuel as well as when gap closure occurs.The methods for simulating each condition are outlined throughout this report.

A $UO_2$ fuel pellet was used for these simulations due to being a traditional form of nuclear fuel. The gap was assumed to be entirely Helium, however it is possible for there to be Xenon in the gap as well, just not for this application. The cladding used was Zirconium, due to its ability to be used in light water reactors (LWRs). The material properties of each material are listed below.

| | Thermal Conductivity | Specific Heat | Density |
|---|---|---|---|
| **Fuel ($UO_2$)** | 0.03 W/(cm·K) | 0.33 J/(g·K) | 10.98 g/cm$^3$ |
| **Gap (He)** | $1.53 \times 10^{-3}$ W/(cm·K) | 5.1932 J/(g·K) | $1.786 \times 10^{-4}$ g/cm$^3$ |
| **Clad (Zr)** | 0.17 W/(cm·K) | 0.35 J/(g·K) | 6.5 g/cm$^3$ |

Table 1: This figure shows the material properties used in the MOOSE programs for the fuel, gap, and cladding.[1][7][3]

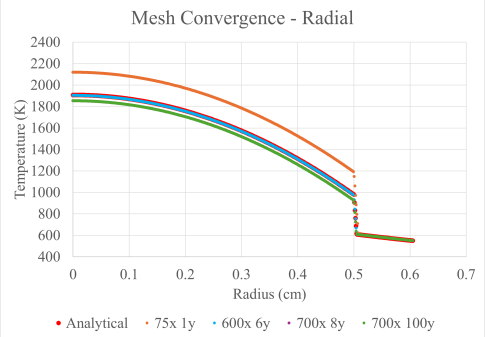


Figure 2: This figure shows the results of the Mesh Convergence test compared to the analytical results.

## Methodology

## Analytical Solution

The analytical solution was calculated using different simplifications of the overall heat conduction equation to form equations for the temperature in the fuel, gap, and cladding. The steady-state LHR with constant thermal conductivity was the only solution able to be tabulated analytically, which is what was used to determine the mesh in each program moving forward. The analytical solution is graphed using Excel, with commands determining which equation is applied to which section. Equations used are outlined in the Equations section of this report.

## General Properties for Defining Programs

Some properties of these separate scenarios are applicable across both steady-state and transient functions regardless of thermal conductivity temperature-dependence. Those properties consist of the mesh, preconditioning, variables, and boundary conditions. Axial conditions are the same as steady-state with temperature-dependent thermal conductivity, with some small changes that will be called out throughout this report.

### *Mesh Determination*

The xmin and ymin are determined by the coordinate (0,0), the bottom corner of the fuel rod pellet, and the xmax and ymax are the outer dimensions of the top right corner of the fuel rod pellet cross section, containing the radius of the fuel pellet (0.5 cm), gap thickness (0.05 cm) and cladding thickness (0.1 cm), (0.605, 1, 0) for the radial temperature profile simulations, and (0.605, 100, 0) for the axial temperature profile simulations. The 2-dimensional nature and geometry are represented by dim = 2 and coord-type *RZ*.

Subdomain1 creates a box around the fuel and the gap, and subdomain2 creates a box around the fuel itself. This forms three boxes; an outer box from the outer part of subdomain1 to the xmax and ymax representing the cladding, a central box between subdomain1's outer limits and subdomain2's outer limits representing the gap, and a left-oriented box between the origin and subdomain2's outer limits representing the fuel. Block ID *2* is associated with the fuel component, Block ID *1* with the Gap, and Block ID *0* with the Cladding.

Mesh nx and ny were determined using a mesh convergence analysis comprised of a series of tests comparing results of the temperature profile of the steady-state LHR with constant thermal conductivity to its corresponding analytical solution. The parameters contributing to creating the temperature profile of the static LHR with constant thermal conductivity component are outlined further along in this report. Figure 2 displays the effect of mesh size on quality of analysis. Using a coarser mesh such as nx=75 and ny=1, the temperature profile reported slightly higher values than the analytical solution, and a finer mesh such as nx=700 and ny=100 reported slightly lower values than the analytical solution and had an extended run time that was inefficient. The mesh corresponding most closely with the analytical solution was nx=600 and ny=6.

When an axial LHR is taken into consideration, a separate mesh convergence test must be executed.

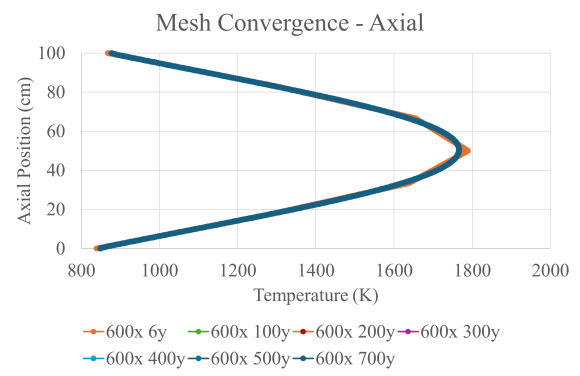


Figure 3: Figure shows centerline temperature profiles of different mesh conditions.

Using several different y-value mesh sizes, it can be determined the smallest mesh that will yield the most accurate value. The centerline temperature profile was taken into consideration for this model. The max temperature and its corresponding axial position converge at approximately 1766.2 Kelvin and 50.50 cm, respectively. The smallest mesh size to achieve these values occurred when ny=200. This optimizes both accuracy and run time of each simulation.

Table 2: Temperature and Axial Position Across Meshes

| Mesh | 6y | 100y | 200y | 300y | 400y | 500y | 700y |
|---|---|---|---|---|---|---|---|
| Max T (K) | 1788.8 | 1766.1 | 1766.2 | 1766.2 | 1766.2 | 1766.2 | 1766.2 |
| Axial Pos. (cm) | 50.10 | 50.90 | 50.50 | 50.50 | 50.50 | 50.50 | 50.50 |

The mesh convergence for the third part of the simulations including burnup dependence was performed by testing different mesh conditions and the resulting maximum stress. The hoop stress condition is used for the maximum value due to it representing the greatest stress inside the cladding and it is important to overestimate these conditions opposed to underestimation for safety purposes. Mesh size was only altered in the x direction, and the y direction values were kept from previous mesh convergence studies throughout these simulations.

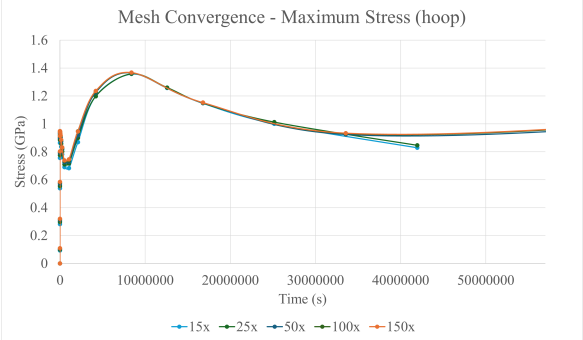


Figure 4: Figure shows maximum hoop stress of different mesh conditions.

The mesh conditions chosen for this application were a mesh of 50x for the fuel and cladding and 20x for the gap. The gap required a smaller mesh due to the smaller region. These values were chosen based on the results of the mesh convergence analysis, showing that the smallest mesh tested yielding statistically significant results was 50x.

### *Preconditioning*

The preconditioning system in MOOSE allows a user to define the type of preconditioning matrix to build (type of system of equations to apply). The Preconditioning system chosen for this application is a solve type of *NEWTON*. Newton's method applies a full Jacobian to the solve to the system and is allows for greater convergence especially in nonlinear situations. It is easier for smaller applications due to the greater stored memory compared to *PJFNK* which was the solve type this program was originally attempted with.

### *Kernels*

Kernels are used to solve pieces of the residual heat conduction equation in the form of a partial derivative. In the steady-state case, two kernels are used; *HeatSource* and *ADHeatConduction*. In the heat source segment, block 2 is identified as the heat source, which corresponds with the fuel pellet. The variable T is then associated with the heat source as a function changing by means of LHR. In the steady state, the LHR is constant, the highest temperature exists at the fuel centerline (radius = 0) and the lowest temperature is on the outer cladding (radius = max). *ADHeatConduction* is used opposed to *ADHeatConduction* due to the automatic differentiation (AD) that is able to compute derivatives of each temperature dependent property per iteration. The heat conduction

variable is used to incorporate the diffusion term of the heat equation, once again denoting temperature as the associated variable. The heat conduction kernel is useful for steady-state and transient heat conduction as well as temperature-dependent thermal conductivity.

In the transient simulation, the *ADHeatConductionTimeDerivative* kernel is added. The time derivative serves to make adjustments to each of the parameters declared, in this case temperature, over each time step. This allows for the formation of a temperature profile over a series of timesteps.

***Postprocessor***

A VectorPostprocessor is used for both steady-state programs. It is set up to take 500 points between declared start/end points, which are along the centerline of the fuel. Each point is paired with the value of the temperature variable. The *sortby* option is used to order the values from least to greatest. This is consistent for both the constant and variable thermal conductivity programs.

The postprocessor used for the transient LHR uses the *PointValue* function to measure the simulated temperature at each timestep to count as a data point each iteration.

Axial LHR simulations use the same postprocessor as steady-state programs, but are altered to be taking values along the y-axis rather than the x-axis. Burnup dependent thermal conductivity simulations use the *ElementExtremeValue* and *ElementAverageValue* to output maximum and average values and the *AxisymmetricCenterlineAverageValue* for centerline specifically. *SideAverageValue* and *DifferencePostprocessor* are used to calculate the gap width as it changes as a function of cladding and fuel thermal expansion simultaneously.

***Executioner***

Executioner type should be steady for steady-state programs. The difference between the constant and variable thermal conductivities is that the variable thermal conductivity program requires additional parameters to help it converge. Nonlinear and linear relative/absolute tolerances are determined through trial and error to find the maximum decimal places the function can converge to in a reasonable duration of time with adequate accuracy.

The transient LHR executioner is the same as steady-state for the constant thermal conductivity section. For the variable thermal conductivity, the *TimeStepper* function block type *IterationAdaptiveDT* was added to further optimize the block. This starts with a smaller time step and after the optimal iterations can adjust to speed up or slow down the simulation time.

The burnup condition executioner uses many similar concepts from the previous applications but applies a petsc option in the solver to provide a stable solution.

***Outputs***

Exodus is the function used in outputs that stores simulation results, and should be marked as true. Then to tabulate data and manipulate for further analysis, it can be exported to a CSV file and named, all is typed in the output block.

The only difference between the steady-state and transient programs output file is the steady-state executes on the final iteration, where the transient executes when it converges after each timestep.

## Materials

***Constant Thermal Conductivity***

Three separate materials were used for these programs, the fuel ($UO_2$), Gap (He), and Cladding (Zr). In the steady-state process with a constant thermal conductivity, the materials were more simple, only requiring the constant thermal conductivity to be declared (each value for thermal conductivity is an accepted value). To differentiate which block is which, there is a block declaration. The type of material for each is an *ADHeatConductionMaterial* because the thermal conductivity is being considered and contributes to a function to determine temperature at each point in the fuel pellet.

Transient LHR with constant thermal conductivity uses a similar Materials block as the steady-state LHR with constant thermal conductivity, except it requires the declaration of thermal conductivity, specific heat, and density. Each were acquired through accepted values. For these blocks, an *ADGenericConstantMaterial* function was used. This is useful for declaring material properties that do not have temperature dependence, so it could have been used for the steady-

state LHR with constant thermal conductivity as well. This function will not be effective for the programs with a temperature dependent thermal conductivity, and more creative solutions are required to declare material properties when some are temperature dependent and others are not.

***Variable Thermal Conductivity***

The fuel, gap, and cladding are declared as *ADHeatConductionMaterials* consistent with each iteration of programs. The difference is that thermal conductivity is in terms of a function. The functions for thermal conductivity are shown in the *Equations* portion of this report. The nomenclature for the function uses *t*, although *t* is indicative of temperature rather than time, this is because the operator must use functions of t or linear coordinates, and through trial and error, *t* was the most functional operating variable. A minimum temperature of 550 Kelvin is also noted so that the function can converge easily.

For the transient LHR with a variable thermal conductivity program, *ADHeatConductionMaterial* functions are used to declare the thermal conductivity temperature and specific heat functions/values. This is because they are considered temperature dependent in MOOSE, whereas densities are treated as constant or a predefined function in MOOSE, and are included in *GenericConstantMaterial* function blocks.

The burnup condition simulation includes elasticity for the fuel, gap, and cladding, with Young's Modulus and Poisson's Ratio defined, and thermal expansion for the fuel and cladding including a thermal expansion coefficient.

| | **E (Pa)** | $\nu$ | $\alpha$ **(1/K)** |
|---|---|---|---|
| **Fuel ($UO_2$)** | $2 \times 10^{11}$ | 0.345 | $11 \times 10^{-6}$ |
| **Clad (Zr)** | $8 \times 10^{11}$ | 0.41 | $7.1 \times 10^{-6}$ |

Table 3: This figure shows additional material properties used in the MOOSE programs for the fuel, gap, and cladding.[5][6]

Lastly, in the materials blocks are computed variables for fuel swelling strain due to densification, thermal expansion, and fission product, both solid and gaseous. This are used through ComputeThermalExpansionEigenstrain and ComputeLinearElasticStress blocks.

## Equations

### Temperature Distribution

The following equations describe the temperature distribution for the fuel, gap, and cladding, along with the average volumetric heat rate (VHR):

$$T_F(r) = \frac{Q_{\text{avg}}(R_f^2 - r^2)}{4k_f} + T_{F0} \tag{1}$$

$$T_G(r) = T_{CI} - \ln\left(\frac{r}{R_g}\right)\frac{LHR}{2\pi k_g} \tag{2}$$

$$T_C(r) = T_{CO} - \ln\left(\frac{r}{R_c}\right)\frac{LHR}{2\pi k_c} \tag{3}$$

$$Q_{\text{avg}} = \frac{LHR}{\pi R_f^2} \tag{4}$$

$$T_{\text{cool}} - T_{\text{cool}}^{\text{in}} = \frac{1}{1.2}\frac{Z_o \times LHR^o}{\dot{m}C_{PW}} \tag{5}$$

$$\times \left\{\sin(1.2) + \sin\left[1.2\left(\frac{z}{Z_o} - 1\right)\right]\right\} \tag{6}$$

Equations describing the temperature distribution. $T_F(r)$ is the fuel temperature, $T_G(r)$ is the gap temperature, $T_C(r)$ is the cladding temperature, $T_{F0}$ is the fuel centerline temperature, $T_{CI}$ is the inner cladding temperature, $T_{CO}$ is the outer cladding temperature, $k_f$ is the fuel thermal conductivity, $k_g$ is the gap thermal conductivity, $k_c$ is the cladding thermal conductivity, $R_f$ is the fuel pellet radius, $R_g$ is the gap radius, $R_c$ is the cladding thickness, $Q_{\text{avg}}$ is the average VHR, $LHR$ is the linear heat generation, and $r$ is the radial position.

—

### Volumetric Heat Rate

The following equations provide conversions from linear heat rate (LHR) to volumetric heat rate (VHR) in both steady-state and transient conditions:

$$VHR_{\text{linear}} = \frac{LHR}{\pi R_f^2} \tag{7}$$

$$VHR_{\text{transient}} = \frac{LHR \times \exp\left(-\frac{(t-20)^2}{2}\right) + LHR}{\pi R_f^2} \tag{8}$$

$$VHR_{\text{axial}} = \frac{LHR^o \times \cos\left(1.2 \times \left(\frac{y}{Z_o} - 1\right)\right)}{\pi R_f^2} \tag{9}$$

figureConversions from linear heat rate (LHR) to volumetric heat rate (VHR). $R_f$ represents the fuel pellet radius and $t$ is time.

—

### Thermal Conductivity

The following equations describe how temperature influences the thermal conductivity for different materials:

### Fuel ($UO_2$)

$$k(T) = \frac{1}{100}\left(\frac{100}{7.5408 + 17.629\left(\frac{T}{1000}\right) + 3.6142\left(\frac{T}{1000}\right)^2} \tag{10}$$

$$+ \frac{6400}{\left(\frac{T}{1000}\right)^{5/2}} \exp\left(\frac{-16.35}{T/1000}\right)\Bigg) \tag{11}$$

### Gap (Helium)

$$k(T) = 16 \times 10^{-6} \times T^{0.79} \tag{12}$$

### Cladding (Zirconium)

$$k(T) = \frac{8.8527 + 7.0820 \times 10^{-3}T + 2.5329 \times 10^{-6}T^2 + \frac{2.9918 \times 10^3}{T}}{100} \tag{13}$$

Thermal conductivity equations for different materials: $UO_2$ fuel, helium gap, and zirconium cladding. $T$ is the temperature, and $k$ is the thermal conductivity in W/cm $\cdot$ $K$.

—

### Heat Conduction

This section outlines the steady-state and transient heat conduction equations:

$$\textbf{Steady-state: } \nabla \cdot (k\nabla T) = Q \tag{14}$$

$$\textbf{Transient: } \rho C_p \frac{\partial T}{\partial t} = \nabla \cdot (k\nabla T) + Q \tag{15}$$

Heat conduction equations for steady-state and transient conditions. $\rho C_p$ is the thermal inertia, where $\rho$ is the density, $\frac{\partial T}{\partial t}$ is the rate of temperature change over time, $\nabla \cdot (k\nabla T)$ is the heat flux divergence, and $Q$ is the volumetric heat source.

### Burnup

$$\beta = \frac{\left(\frac{\text{VHR}}{E_f}\right) \cdot t}{N_U} \tag{16}$$

### Fission Products

### Thermal Expansion Strain

$$\varepsilon_{\text{th}} = \int_{T_{\text{ref}}}^{T} \alpha(T')\, dT' \tag{17}$$

### Densification Strain

$$\epsilon_D = \Delta\rho_0 \left(e^{\frac{\beta \ln 0.01}{C_D \beta_D}} - 1\right)$$

$$C_D = \begin{cases} 7.235 - 0.0086(T(^\circ\text{C}) - 25), & \text{for } T < 750^\circ\text{C} \\ 1, & \text{for } T \geq 750^\circ\text{C} \end{cases}$$

$$\epsilon_D = \Delta\rho_0 \left(e^{\frac{\beta \ln 0.01}{C_D \beta_D}} - 1\right)$$

### Solid Fission Product Swelling

$$\varepsilon_{\text{sfp}} = f(\beta, \rho) \tag{18}$$

### Gaseous Fission Product Swelling

$$\varepsilon_{\text{sub gfp}} = 1.96 \times 10^{-28} \cdot \rho \cdot \beta \cdot (2800 - T)^{11.73} \tag{19}$$

$$\cdot\, e^{-0.0162 \cdot (2800 - T)} \cdot e^{-17.8 \cdot \rho \cdot \beta} \tag{20}$$

### Cracking

$$\sigma_{\theta\theta}(\eta) = -\sigma^*(1 - 3\eta^2)$$

$$\sigma^* = \frac{\alpha E(T_0 - T_s)}{4(1 - \nu)}$$

$$\eta = \frac{r}{R_f}$$

## Results

### Steady-State Linear Heat Rate

The figure below shows how the temperature profile of a steady-state LHR presents itself. A maximum temperature can be observed in the centerline of the material (radius = 0 cm), which makes sense when comparing to literature expectations, as well as the analytical solution. The constant thermal conductivity curve yielded a slightly higher centerline temperature of 1900 K, whereas the variable thermal conductivity curve yielded a centerline temperature of 1750 K.

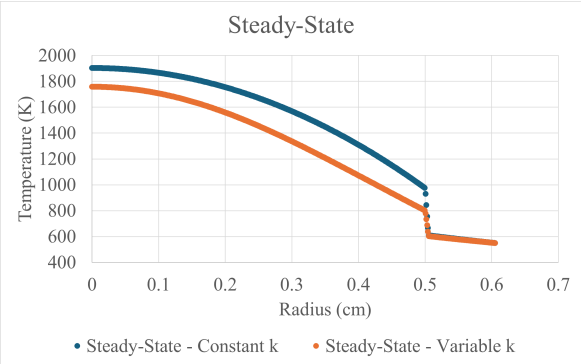


Figure 5: This figure shows the results of the steady-state LHR programs, comparing the temperature profile resulting from a constant vs a variable thermal conductivity.

The largest change between the constant and variable thermal conductivity scenarios is attributed to the gap. The constant thermal conductivity temperature profile experiences a much larger change in temperature across the gap. This is due to as the radius becomes closer to the centerline, the gap becomes hotter, causing the thermal conductivity to increase, and conduct heat away from the fuel faster. The fuel segment shape of the constant vs the variable thermal conductivity are similar, they are just offset due to the larger gap temperature change when assuming a constant thermal conductivity.

### Transient Linear Heat Rate

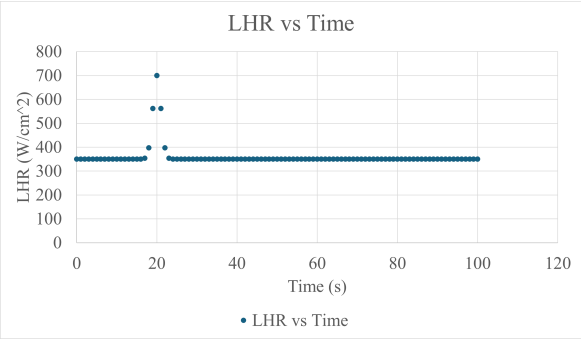


Figure 6: This figure shows the fluctuation of LHR based on the function provided.

It can be observed that the peak in the transient temperature profile is at about the same timestamp as the LHR vs Time plot peaks. This suggests a relationship with LHR increase and temperature spikes over time, there is an initial sharp increase in temperature as the power input in the LHR is increased and once the heat generation equals heat removal, thermal equilibrium is established and the system reaches steady-state, when the curve flattens out.

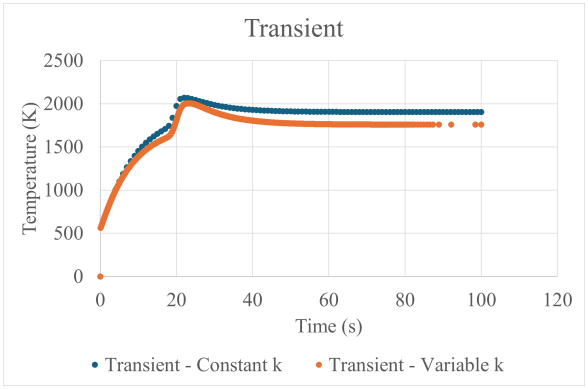


Figure 7: This figure shows the results of the transient LHR programs, comparing the temperature profile resulting from a constant vs a variable thermal conductivity.

### Axial Linear Heat Rate

Temperature profiles using an Axial LHR are at a maximum at approximately the center of the fuel rod are shown in the figure below.

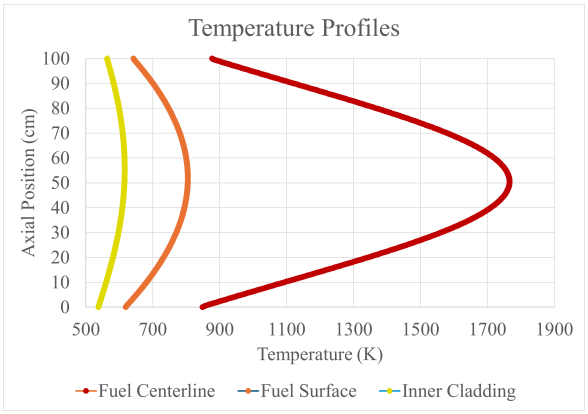


Figure 8: Displays the axial temperature profiles of the fuel centerline (red), fuel surface (orange), and outer cladding (green).

The temperature profiles all follow parabolic patterns, with the fuel centerline having the highest peak temperature. The gap in temperature between each section changes as a function of axial position due to the change in thermal conductivity as the temperatures change, causing the center of the fuel rod (radially and axially) to become exponentially hotter than the rest of the fuel centerline, surface, and cladding.

Table 4: Max Temperature and Axial Position

| Profile | T (K) | Ax. Pos. (cm) |
|---|---|---|
| Fuel Centerline | 1766.2 | 50.50 |
| Fuel Surface | 804.8 | 51.90 |
| Inner Cladding | 616.3 | 55.51 |

The maximum temperatures of each of the analyzed regions are listed in the table above, as well as their corresponding axial positions. The inner cladding maximum temperature was 5.5 cm above the axial midpoint, and as the radial position becomes closer to the center, the maximum temperature occurs more towards the midpoint, settling 0.50 cm above the midpoint at the centerline.

### Linear LHR with Temperature and Burnup dependent Thermal Conductiviy

*Displacement vs. Time*

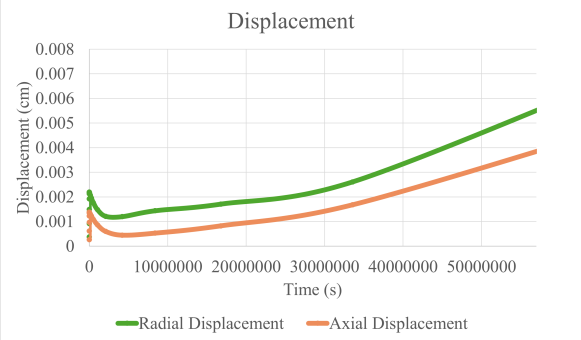


Figure 9: Plot of Displacement in the axial and radial directions as a function of time throughout the fuel cycle

*Gap Width vs. Time*

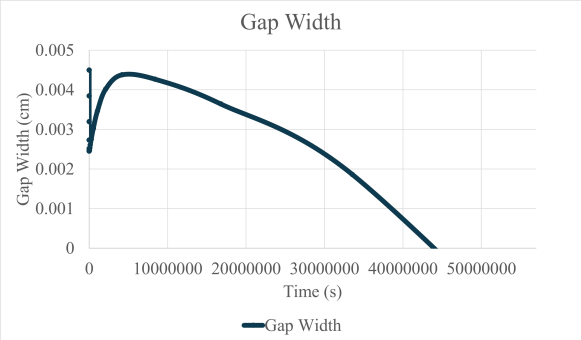


Figure 10: Plot of the change in gap width as a function of time throughout the fuel cycle

To be noted on both the displacement and gap width plots is an initial spike, before decreasing. The displacement plot shows the same behavior but a higher degree of radial displacement compared to axial. When the gap width approaches zero, both the displacement and gap width trends are linear.

*Maximum Stress vs. Time*

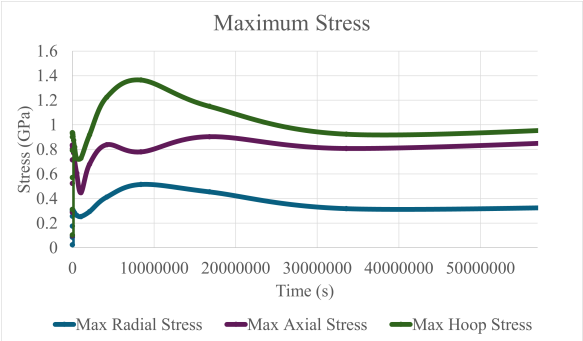


Figure 11: Plot of maximum stress in the radial and axial directions and hoop stress as a function of time throughout the fuel cycle

*Average Stress vs. Time*

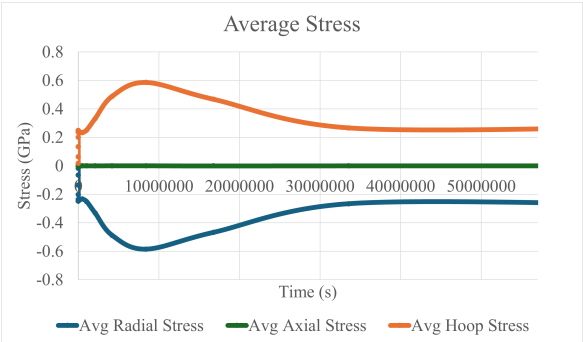


Figure 12: Plot of average stress in the radial and axial directions and hoop stress as a function of time throughout the fuel cycle

The average and maximum stresses peak at similar positions, and in each case the hoop stress is the largest, followed by axial, then radial stress. The stress values become constant just before the gap closure occurs.

## Discussion

The lower temperature profiles observed in the constant thermal conductivity plots versus the steady-state temperature profiles can be attributed to the overall increase in thermal conductivity with temperature. A higher thermal conductivity means a greater amount of heat is leaving the fuel pellet, at a higher rate. this leads to the slightly steeper

gradient and the higher average temperature profile when k is unchanging. At higher temperatures, heat is conducted more efficiently and the centerline temperatures will decrease when the thermal conductivity is a function of temperature.

The importance behind studying both steady-state and transient behavior is to show a stable temperature profile to use for long term operation and understanding burn-up of individual fuel rods based on temperature, which can help logically configure fuel rods for the most efficient operation. Transient profiles show the response to changes in power, in this case LHR. It is important to understand the difference between variable and constant thermal conductivity as well, because the variable is more accurate as to what is occurring in the fuel rod, but constant can make for more straight forward assumptions. However, it is necessary to note that using a constant k would result in a consistent overestimation of temperature regardless of which case is being looked at.

Axial temperature profiles of areas of interest inside of a fuel rod have been analyzed before. The figure below contains results from an experiment performed by INL, using cold, un-irradiated fuel thermal conductivity and dimensions. The MOOSE simulation does not yet take into consideration fuel swelling and uses temperature-dependent thermal conductivity opposed to a similar "cold" assumption, but the overall behavior is comparable.

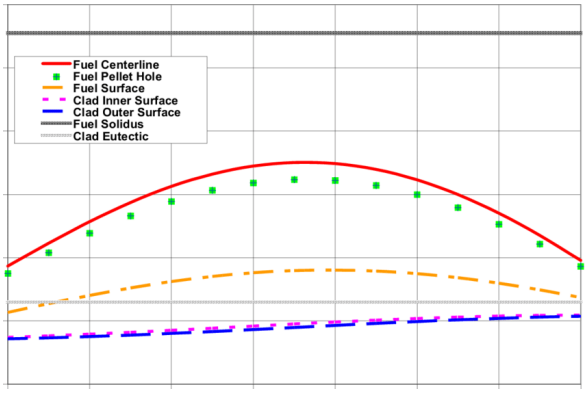


Figure 13: Axial temperature distributions calculated in the hot channel: bulk coolant, cladding inner and outer surface, fuel surface and fuel centerline temperatures. [2]

INL's plot validates the results from the axial MOOSE simulation. The change in peak temperatures between the fuel centerline, fuel surface, and fuel inner cladding are of a similar scale to the results from this simulation. It is also important to note that according to these plots, the maximum temperature is slightly above the midpoint of the fuel rod, which aligns with MOOSE results.

The maximum temperature may be slightly above the centerline of the fuel due to the coolant losing heat as it flows up along the fuel rod, and its ability to remove heat from the system decreases, causing a biased parabolic shape. This is shown in the following figure. The coolant profile acts as an outer boundary condition that alters the temperature profile within.

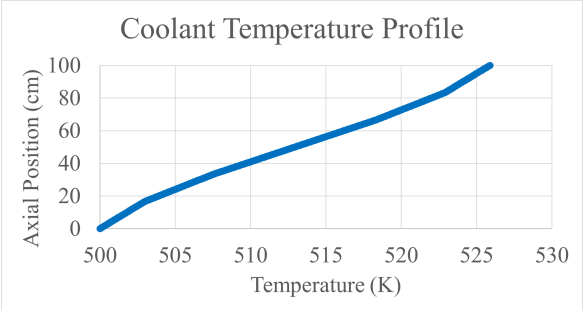


Figure 14: This figure shows axial temperature profile of the coolant.

The results listing the maximum temperature at different radial locations such as the fuel centerline, fuel surface, and inner cladding show that the maximum temperature occurs at a higher axial position if it is being measured at a greater radial distance from the centerline. This is because as the coolant loses its ability to remove heat, an initial gradient is formed at the outer cladding, resulting in different thermal conductivities at the midpoint and the ends of the inner cladding. This affect is greatest at the coolant/cladding interface, but slowly is mitigated as the radial position approaches the centerline.

It is also interesting to see that near the top and bottom of the fuel rod, the differences in temperature of the fuel centerline/surface and cladding are lesser, which is due to the centermost point of the fuel being the hottest and the ends being cooler. This is validated by many simulation techniques and by loss of coolant accidents (LOCAs) which causes the midpoint of the fuel rod to fail and burst first.

The temperature and burnup dependent thermal conductivity simulation yields several different results. First off, radial displacement has the same shape as axial displacement, but is smaller. This is because of the temperature gradient and pressure distribution within the fuel rod. Fission gas bubbles move outwards towards the coolant, and the quickest path is towards the outward cladding, resulting in a greater radial displacement.

One of the noteworthy points on the plots are the spikes at the beginning of the displacement, gap width, maximum stress, and average stress plots. The initial spike indicates the rapid heating and swelling of the fuel due to thermal effects. The maximum stress and average stress plots experience a second spike towards the midpoint which is indicative of the radial cracking and creep behavior of the fuel, which causes the displacement curve to slightly flatten. The displacement curve then increases in slope again once the gap closure occurs as shown on the gap width plot.

Pellet cladding interaction (PCI) occurs when the gap width = 0. This occurs after approximately 57740000 seconds (668 days) of use. As the gap closure occurs, the stresses become more linear, although this does not accurately represent the fuel behavior after the gap closes entirely. Radial stresses are often negative, due to the bamboo-ing effect of the fuel pellet, which is when there are large thermal gradients radially, less so axially, which contribute to non-uniform expansion.

| **Max Stress (GPa)** | $\Delta T$ **(K)** | $\sigma^*$ **(GPa)** | $\eta$ | **r (cm)** |
|---|---|---|---|---|
| 1.3652 | 1122.7962 | 6.4718 | 0.6353 | 0.3177 |

For this simulation, the crack depth is calculated using the maximum stress (hoop stress) conditions and is approximately 0.32 cm. Fracture stress occurs around when $\eta = 0.65$, which is approximately where this simulation maximizes at, showing that the material has fractured. Crack morphology and behavior is not taken into consideration in this model, in the future it is important to understand crack propagation and how that will affect modeling the fuel behavior. It is important to note that cracking occurs within the fuel before PCI, due to the high concentration of stresses from fission products, densification, and thermal expansion. After cracks are initiated, the fuel is able to deform and expand under even higher stresses before failure, similar to a tensile test, how there is an elastic yield strength before deformation.

## Conclusion

Using a fuel pellet consisting of $UO_2$ fuel, entirely Helium gap, and a Zirconium cladding, the maximum centerline temperatures for each condition are cited in the following table.

Table 5: Maximum Centerline Temperatures

| **LHR Type** | **Thermal Conductivity** | **T (K)** |
|---|---|---|
| Steady-state | Constant | 1903 |
| Steady-state | T-dependent | 1758 |
| Transient | Constant | 2070 |
| Transient | T-dependent | 2005 |
| Axial | T-dependent | 1766 |

The temperature dependent thermal conductivity curves were collectively lower than the constant thermal conductivity curves for both steady-state and transient due to the higher net thermal conductivity in the gap and cladding conducting heat out of the fuel pellet. A transient linear heat rate results in a peak centerline temperature at about the 20-23 second timestep due to the spike in LHR at that time from the transient LHR equation. It is important to simulate each of these situations to understand fuel at different linear points throughout the fuel pellet and after different lengths of time in the reactor. This helps predict fuel behavior and ensure safe operation of nuclear reactors. The axial variation of the power input LHR0 also causes the variations within the temperature profile.

Axial temperature profiles show where the maximum temperature occurs as a function of axial position. The position is slightly above the midpoint of the fuel rod which is due to the change in coolant thermal conductivity as it flows from the bottom to the top of the fuel. The center of the fuel is exponentially hotter than the ends, making it more susceptible to incidents such as LOCAs.

Burnup-dependent stress profiles and gap width changes allow the crack depth to be determined, as well as the timeline of the stage of the high burnup structure. The peaks of the plots represent the behavior of the fuel due to thermal expansion and crack propagation. PCI occurs after about 1 year and 10 months. This is important to know to predict the behavior of fuels. If through cracks occur,

cladding can be penetrated by the coolant which causes an increase in oxidation and hydriding at the inner surface. This can also cause fission products to leak into the coolant. Understanding fuel behavior under specific power and burnup conditions helps determine the time to failure.

## References


[1] Angstrom Sciences. Thermal conductivity of elements, 2025.

[2] Samuel Bays, Rodolfo Ferrer, Michael Pope, Benoit Forget, and Mehdi Asgari. Neutronic assessment of transmutation target compositions in heterogeneous sodium fast reactor geometries, 02 2008.

[3] J. K. Fink and L. Leibowitz. Thermal conductivity of zirconium. *Journal of Nuclear Materials*, 226:44–50, Oct 1995.

[4] Idaho National Laboratory. Moose: Multiphysics object oriented simulation environment, 2025.

[5] Idaho National Laboratory. Nuclearmaterialuo2 action – bison documentation. `https://mooseframework.inl.gov/releases/bison/v2.0.0/source/actions/NuclearMaterialUO2.html`, 2025. Accessed April 25, 2025.

[6] E.B. Schwenk, K.R. Wheeler, G.D. Shearer, and R.T. Webster. Poisson's ratio in zircaloy-4 between 24° and 316°c. *Journal of Nuclear Materials*, 73(1):129–131, 1978.

[7] University of Massachusetts Amherst, Chemistry Department. Appendix: Specific heats, 2025.


## Appendix

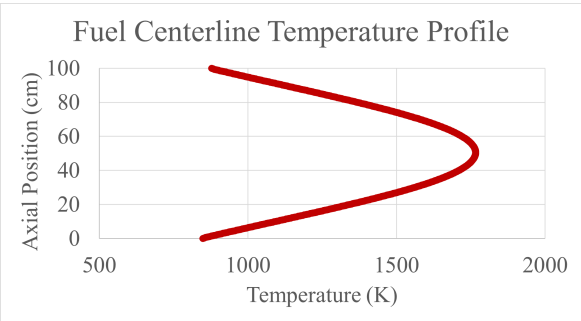


Figure 15: This figure shows axial temperature profile of the fuel centerline.

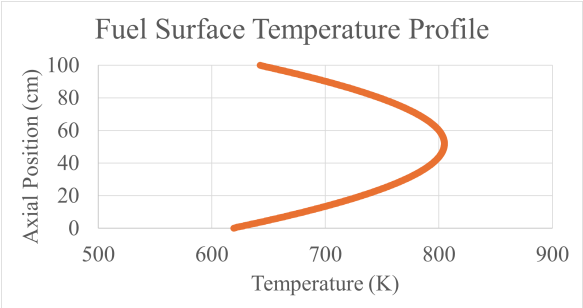


Figure 16: This figure shows axial temperature profile of the fuel surface.

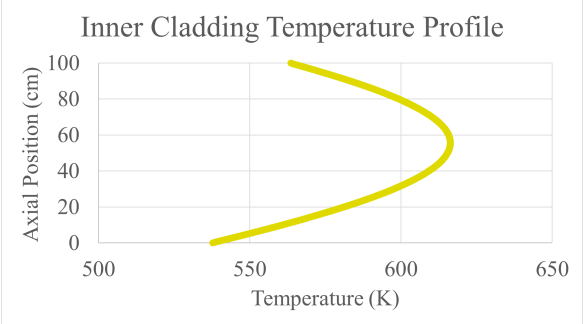


Figure 17: This figure shows axial temperature profile of the inner cladding.

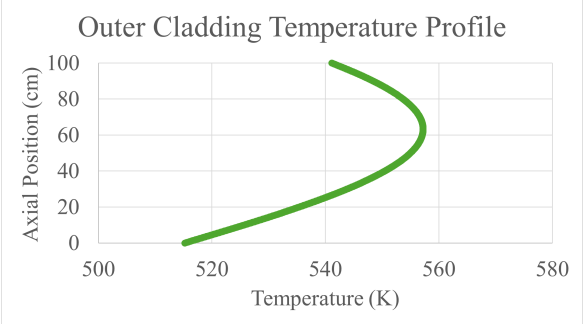


Figure 18: This figure shows axial temperature profile of the outer cladding.